RECURRENT FINE STRUCTURES IN JOVIAN S-BURST EMISSION

B. P. Ryabov*, P. Zarka†, H. O. Rucker‡,
V. B. Ryabov*, and M. Y. Boudjada‡

Abstract

Recent digital observations of Jovian S–emission are presented. They have been performed with high sensitivity (10 Jy) at the Kharkov UTR–2 radiotelescope, using receivers with high time and frequency resolutions (down to 5 ms and 13 kHz, and 2 ms at 30 selected frequencies), over long tracking times (hours) and a broad spectral range ($>10 \div 15$ MHz). Their analysis allows us to constrain the S–bursts source location and radiation pattern as a function of frequency, and to draw information about the geometrical structure of the Io Flux Tube (IFT) and its dynamics. New features of the Jovian S–emission are revealed, related to the evolution of the S–bursts fine structure during storms. Several observed characteristics of S–emission are discussed in the frame of a generation model [Ryabov, 1992, 1994] in which S–bursts are the final product of ruptures of small–scale current filaments circling around the IFT surface, including the overall phenomenology of S–bursts dynamic spectra (complexity as a function of the source observed – Io–B, Io–C, etc. – , evolution of the S–bursts fine structure during storms, occurrence distributed in several spectral sub–bands and their fluctuations and drifts) and morphological details (individual bursts crossing the spectral gap between bands, fixed–frequency durations, dotted patterns in the frequency–time plane, complex fine structures including positive drifts). Special attention is given to repeatable fine structures in the f–t plane, and interpretations are proposed.

1 Introduction

The fine structure of dynamic spectra of the S–component from Jupiter's radio emission ("S" stands for Short–lived bursts, also called "millisecond" radio bursts) has been studied for about forty years [Alexander and Desch, 1984; Bigg, 1964, 1966; Carr et al., 1983; Carr and Reyes, 1992; Desch, 1978; Desch et al., 1978; Dulk, 1970, 1992; Ellis,

*Institute of Radio Astronomy, Ukrainian Academy of Sciences, Kharkov, 310002, UKRAINE
†Observatoire de Paris–Meudon, F-92195 Meudon Cedex, FRANCE
‡Space Research Institute, A-8010 Graz, AUSTRIA

1975, 1979, 1982; Flagg and Desch, 1979; Leblanc et. al., 1980a,b, 1981; Riihimaa, 1977, 1991, 1992; Rucker et. al., 1988, 1992; Warwick et. al., 1979a,b]. High frequency–time (f–t) resolution has been achieved in some observations, but many of them lack either high sensitivity or sufficiently long duration of tracking time (minutes) compared to the average duration of S–burst storms (hours). Recent observations made with the UTR–2 radio telescope in Kharkov have allowed to study the large–scale characteristics of S–burst storms dynamic spectra over a wide range of frequencies (>15 MHz), for long tracking times, above a minimum flux of about 10 Jy [Ryabov et. al., 1985; Ryabov, 1986, 1990a,b, 1992, 1994; Ryabov and Gerasimova, 1990]. Such studies have allowed to constrain the source location and the spectral structure of the S–emission cone radiation pattern, and to draw information about the geometrical structure of the Io Flux Tube (IFT) and its dynamics. A physical model of the S–emission generation mechanism and radiation source has been proposed [Ryabov and Gerasimova, 1990; Ryabov, 1992, 1994], consistent with the angular parameters of the emission cone [Ryabov, 1990b], the derived source location [Ryabov, 1990a, 1996], the planet's magnetic field topology [Connerney et al., 1981; Connerney, 1992, 1993], and the observed fine structures in S–burst dynamic spectra, especially the bursts drift rates in the f–t plane [Ellis, 1979, 1982; Leblanc et al., 1980a,b; Flagg et al., 1991; Riihimaa, 1992; Zarka et al., 1996; Boudjada et al., 1996]. Since 1991, a fruitful cooperation has been established between the Institute of Radio Astronomy (Ukrainian Academy of Sciences) and the Space Research Institute (Austrian Academy of Sciences), devoted to the study of Jovian decametric (DAM) emission at very high f–t resolution. In 1993, the Paris–Meudon Observatory has joined this cooperation. Since then, five observation campaigns of Jupiter have been carried out using Kharkov's UTR–2 radio telescope in conjunction with both an acousto–optical spectrograph (AOS, built in France) and a multichannel digitization system of the 30 UTR–2's analog radio receivers (denoted hereafter MCS for multichannel spectrograph, built in Austria), recently installed at the telescope. This unique combination of the world's largest decameter array UTR–2 with superfast receivers allowed to collect unique (and nevertheless abundant) high–sensitivity / high–resolution digital dynamic spectra of S–bursts in the range $10 \div 30$ MHz, for Io–controlled DAM sources Io–B, Io–C, and Io–A/C. The Kharkov UTR–2 decameter radio telescope [Braude et al., 1978] has an area of 150000 m^2, an (upgraded) operating band $8 \div 30$ MHz, quasi all–sky continuous tracking capability (northern hemisphere), and a multi–beam phasing system allowing to perform simultaneous "On–Off" observations [Zarka et al., this volume]. The minimum detectable flux density varies from 100 to 10 Jy for frequencies in the range $10 \div 25$ MHz. The AOS, which provides f–t resolutions of 13 kHz and 5 ms over a total frequency band of 25 MHz, has been used simultaneously with the MCS, which provides a 2 ms time resolution at 30 selected frequencies. The recorded S–burst dynamic spectra have been processed in order to remove interference (at timescales longer than 1 minute). Adaptative f–t interpolation has been performed to improve the resolution of the observations, assuming a continuous slope for the S–bursts rapidly drifting structures from one spectrum to the next: time resolution of AOS data is thus increased at the cost of redundant frequency resolution, while the MCS spectral resolution is improved at the expense of its very high time resolution. Finally, amplitude transformation is applied to enhance the contrast of weak S–bursts relative to the background (which includes the unavoidable man–made interference).

2 Overall Phenomenology of Jovian S–Burst Dynamic Spectra

The above processed data, sampling the period 1994 ÷ 1996, will be exhaustively presented in the form of a new "Atlas of Jovian Millisecond Radio Bursts" (in preparation). In contrast with earlier S–bursts atlases [Ellis, 1979; Flagg et al., 1991; Riihimaa, 1992], the discussion of high–sensitivity, wide band, and long–lasting observations of S–burst storms which exhibit complex S–burst f–t patterns will be favoured. A large number of S–bursts recorded during this period have indeed very intricate dynamic spectral shapes, while more simple bursts drifting quasi–linearly in the f–t plane actually represent a relative minority of cases. S–bursts drift–rates are generally negative (i.e. the burst frequency decreases with time). However, part of complex bursts actually correspond to positive drifts (Boudjada et al., [this volume]). During an S–burst storm observed from the ground, two stages of complexity in the amplitude–f–t patterns can usually be distinguished, each lasting for a few tens of minutes. The initial stage is dominated by simple bursts of moderate amplitude, displaying a quasi–linear negative drift, and extending over a total frequency range of 2 ÷ 4 MHz with a total lifetime of about 50 ms (Figure 1). The next stage is characterized by an enhanced amplitude and an increased complexity of individual burst shapes (Figure 2). At the end of an S–burst storm, the situation may return to the initial stage. Enhanced f–t resolution, together with the high sensitivity of the telescope, reveal very complex details of the intrinsic S–bursts structure (Figure 3). This fine structure is not always so well defined, and the amplitude distribution in the dynamic spectra sometimes looks much more noisy or random (Figure 4).

After zooming in time, simple S–bursts appear as a stretched "S" letter in the f–t plane (Figure 5), consistent with the adiabatic motion of electron bunches in the Jovian magnetic field [Ellis, 1982; Zarka et al., 1996; Zarka et al., this volume]. Emission at both ends of the S–shaped structure display comparatively short fixed–frequency duration (2 ms), slower drift–rates, and smaller flux densities. Near the burst's center frequency, mid–range of the "S" structure, the fixed–frequency duration increases (up to 15 ms), as well

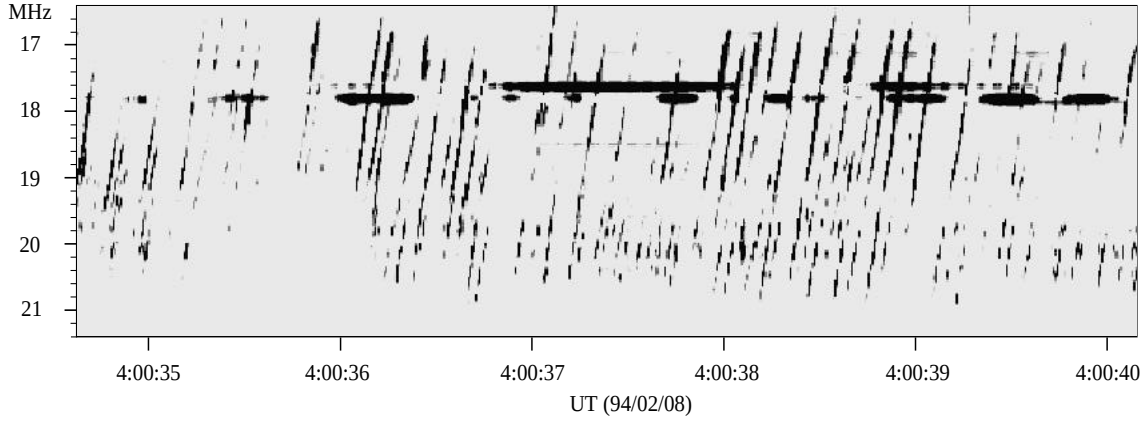

Figure 1: Dynamic spectrum of Jovian Io–B S–emission recorded with UTR–2 + AOS on Feb. 8, 1994, showing simple, quasi–linearly drifting S–bursts. This corresponds to the initial stage of IFT excitation, with yet little distorted magnetic field topology. Note that frequency increases downwards.

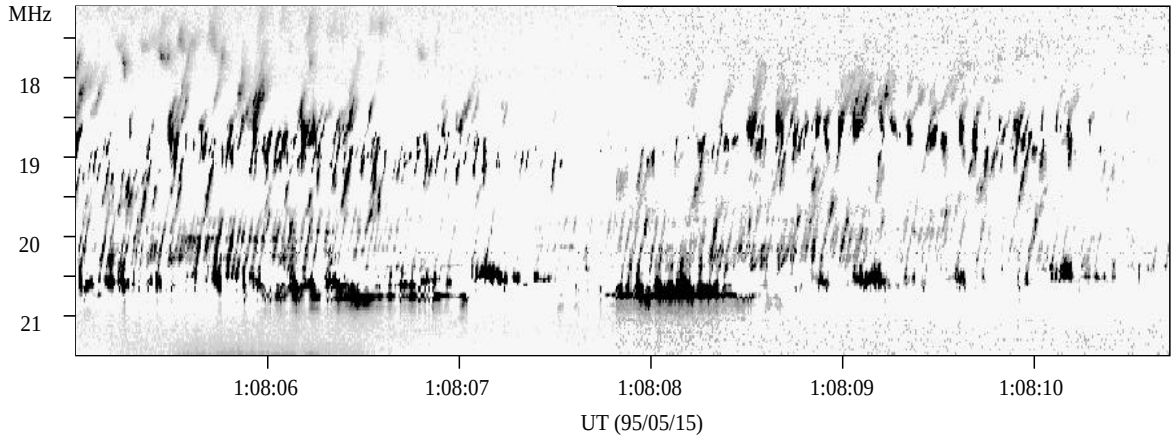

Figure 2: Io–C S–emission recorded with UTR–2 + AOS on May 15, 1995, showing complex S–bursts shapes corresponding to a later stage of IFT excitation than Figure 1 (with strongly distorted magnetic field in the source region).

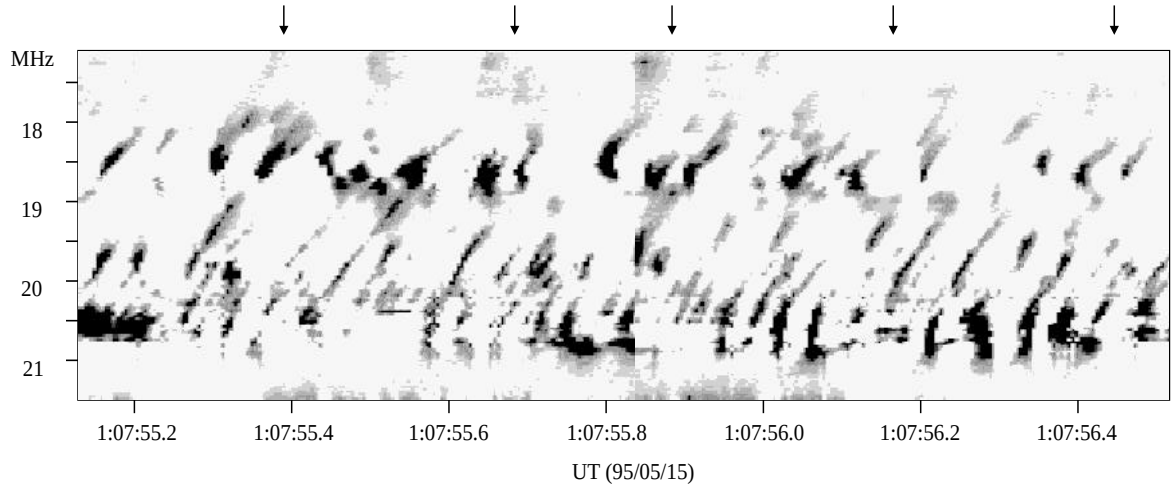

Figure 3: Zoomed dynamic spectrum (with increased time resolution) of the same storm as Figure 2, showing the detailed fine structure and repetitivity of complex S–burst patterns (a recurrent y–like shape is arrowed). The data displayed were recorded 10 seconds before those of Figure 2.

as the drift–rate and flux density. Individual S–bursts have a total frequency bandwidth from about 1 MHz up to 6.5 MHz. S–bursts sequences concentrate within well separated frequency sub-bands, some examples of which are shown in Figure 6. The frequency width of sub–bands evolves over timescales of several minutes. It may vary in the range from 1 to 6 MHz in the course of an S–burst storm. For example, Figure 6a reveals two bursts sub–bands: a narrow one (1 MHz wide) at higher frequencies, about 24 MHz, and a wider one (4 MHz) covering the lower part of the spectrum. Fourteen minutes later, in Figure 6b, three sub–bands can be observed, centered near 16, 20 and 24 MHz, with an opposite width distribution versus frequency: the narrower emission band is at lower frequencies (16 MHz) while wideband S–bursts have moved to higher frequencies. Average sub–band center frequencies are located near 13, 16.5, 20, 23.5 and 27 MHz. S–emission occurrence probability computed over a long time interval maximizes at these frequencies, as shown on Figure 7 [Ryabov et al., 1985]. At timescales of tens of seconds to minutes, however,

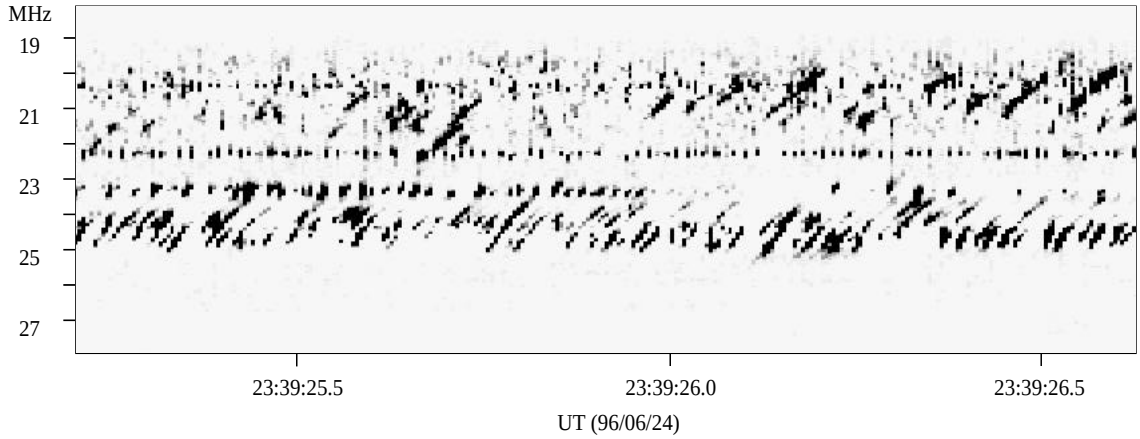

Figure 4: Io–C S–emission recorded with UTR–2 + AOS on June 24, 1996, showing random–like fine structures (especially at low frequencies), which could correspond to an extremely disturbed state of the IFT at the radiating regions.

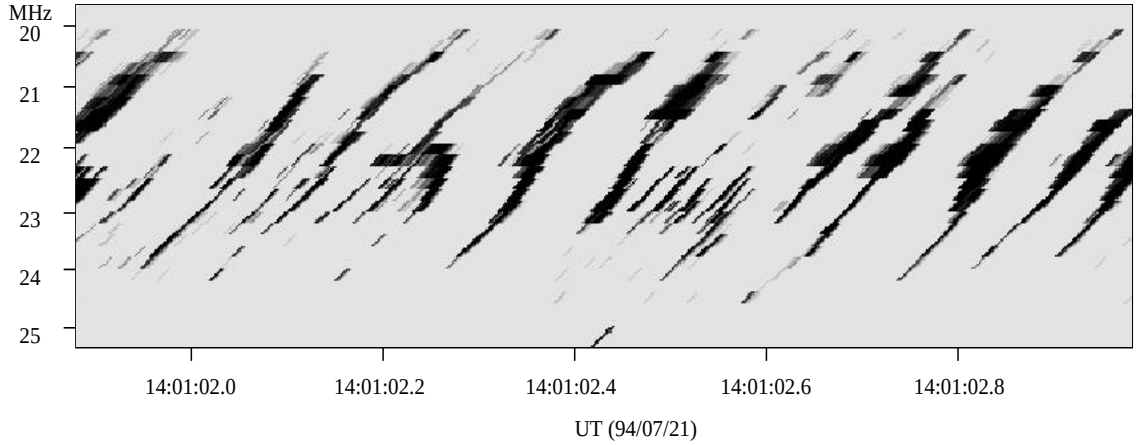

Figure 5: Zoomed dynamic spectrum of quasi–linearly drifting S–bursts (Io–AC source of July 21, 1994) recorded with UTR–2 + MCS, evidencing the S–shape of individual bursts and their variable fixed–frequency duration versus frequency (longer at the center of the burst than at the edges). The Figure shows spectra of changing thickness and drift rate over the f–t plane.

sub–band center frequencies may fluctuate within 1.5 MHz. Our long–lasting observations reveal other details of the S–bursts sub–bands spectral behaviour, as an apparent slow positive frequency drift of these sub–bands $(df/dt)_{sb}$, at an average rate about 1.4 kHz/s on day 94/02/01 (Figure 6 – see also Boudjada et al. [1995]).

3 Detailed Morphology of S–Emission

It is largely supposed that the S–emission source is located in the IFT upward streaming branche(s) [Bigg, 1964; Desch et. al., 1978; Leblanc and Genova, 1981; Ellis, 1982; Alexander and Desch, 1984; Ryabov, 1986]. The Io–Jupiter electric current system, sketched in Figure 8, is non–uniformly distributed and probably sustains a complex spatial structure and temporal dynamics (variability). The Jupiter–Io geometry underlying S–radiation

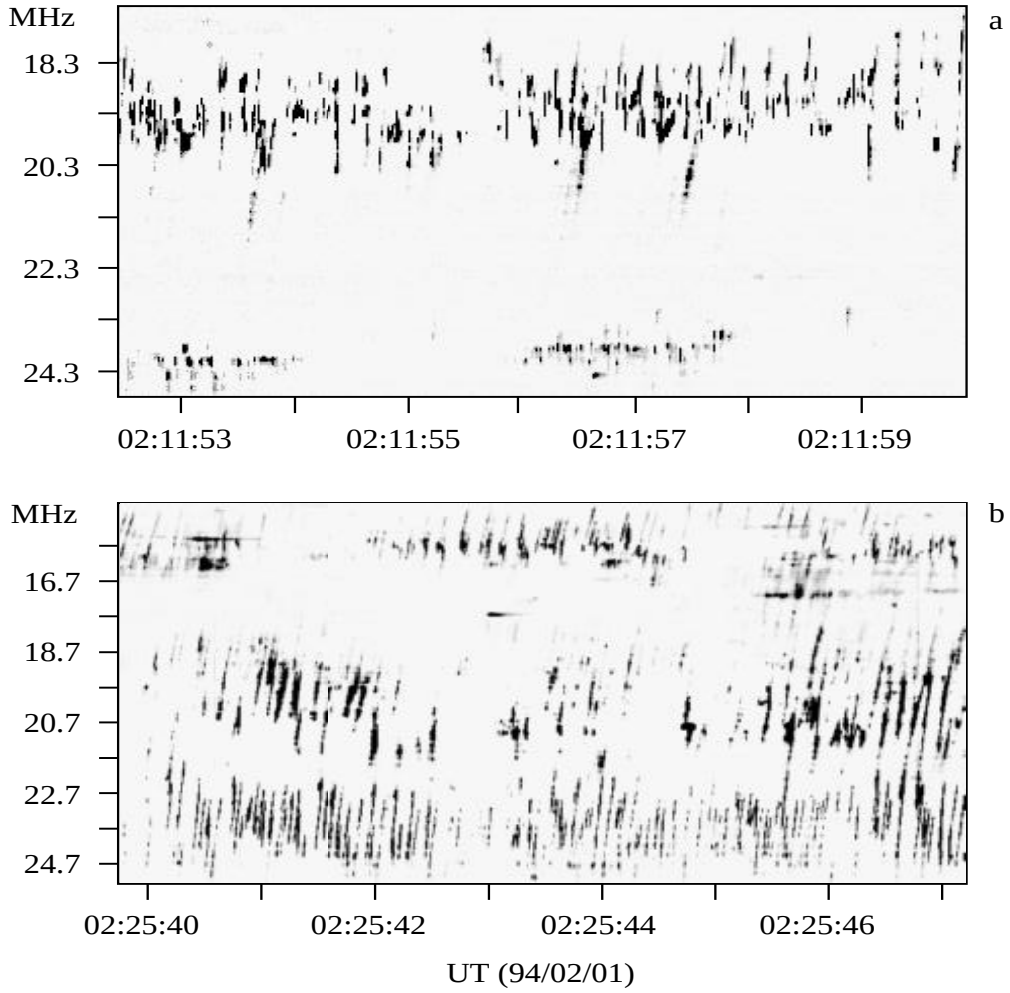

Figure 6: Dynamic spectra of Jovian Io–B S–emission recorded with UTR–2 + AOS on February 1, 1994. S–bursts are grouped in two spectral sub–bands separated by a 3–4 MHz gap in (a). 14 minutes later, during the same storm, the sub–bands spectral width has changed drastically, and a third band has appeared at lower frequencies (b).

is given in Figure 9: locations of the radio emission cones and IFT active intervals are displayed. Their spatial and temporal evolution at timescales of minutes to hours depends on the variations of the Io–Jupiter electric current, and on the local magnetic field strength and topology.

So–called "sources" of Jovian decameter S–emission are usually distinguished according to their location on the observer's longitude in system III (λ_{III}) and Io–phase (Φ_{Io}). This characterizes the motion of the IFT footprint over Jupiter's surface and the observer's location relative to the IFT. Moreover, the IFT itself is warped with respect to the meridian plane, leading to additional complexity in the observed spectral patterns. The S–bursts radiation beam is a hollow cone, with large apex angle and cone axis directed along the IFT at the generation point [Green, 1984; Zarka, 1988], consistent with generation by the cyclotron–maser instability (see e.g. Le Quéau, [1988]). All these characteristics must be taken into account when modelling S–bursts dynamic spectra. The existence of distinct "sources" in the λ_{III} – Φ_{Io} plane is due to the observer intersecting the two opposite

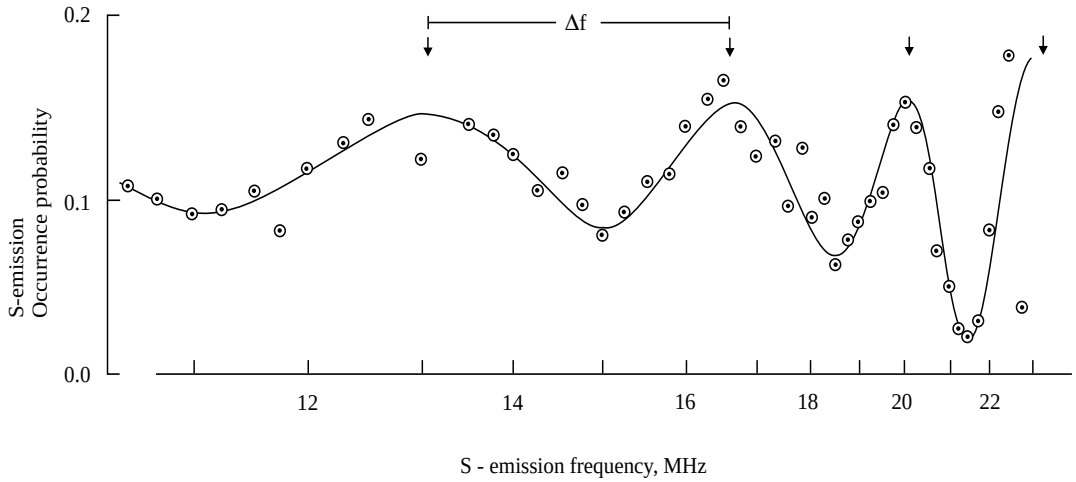

Figure 7: Average S–bursts occurrence probability versus emission frequency, evidencing the sub–bands structure (from Ryabov et al. [1985]).

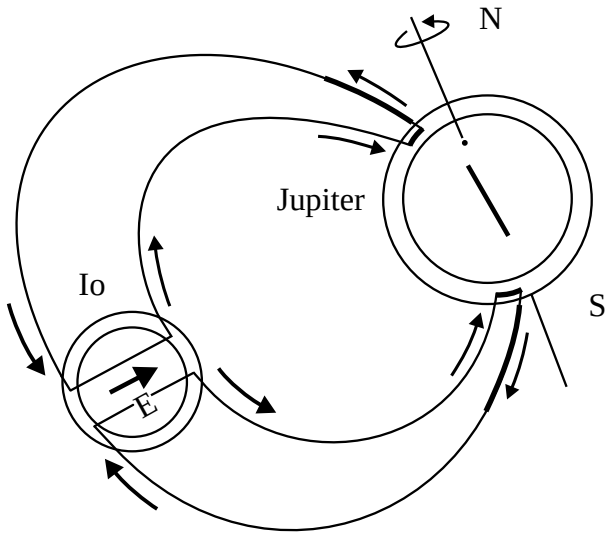

Figure 8: Sketch of the Jupiter–Io current circuit (arrows). S–emission is thought to originate from the upwards streaming IFT branch (boldface).

sides of the hollow emission cone (Io–BD versus Io–AC), and to the variation of the IFT activity when its footprint intersects different active Jovian longitudes (Io–A versus –C, Io–B vs -D). The most versatile morphology of S–bursts f–t patterns corresponds to Io–C configuration, whereas the Io–B one generates the most powerful and comparatively simple bursts. This difference can be attributed to (i) the different geometries of the IFT radio radiation beam with respect to the observer in these two configurations (Io–C corresponds to the observer facing the concave side of the IFT, and Io–B to the observer facing the convex side – in the frame of the 3–D geometry of the O6 field model [Connerney, 1992]), and (ii) to the different longitudes of the IFT footprint on the surface of Jupiter. The IFT footprint trajectory traverses – at high Jovian latitudes – regions of variable

magnetic field strength, and the value of the IFT transverse velocity through the inner Jovian magnetosphere varies itself with the longitude. As a consequence, the S–emission power output, frequency band, polarization, beaming and fine structures change as the footprint moves (see subsequent section).

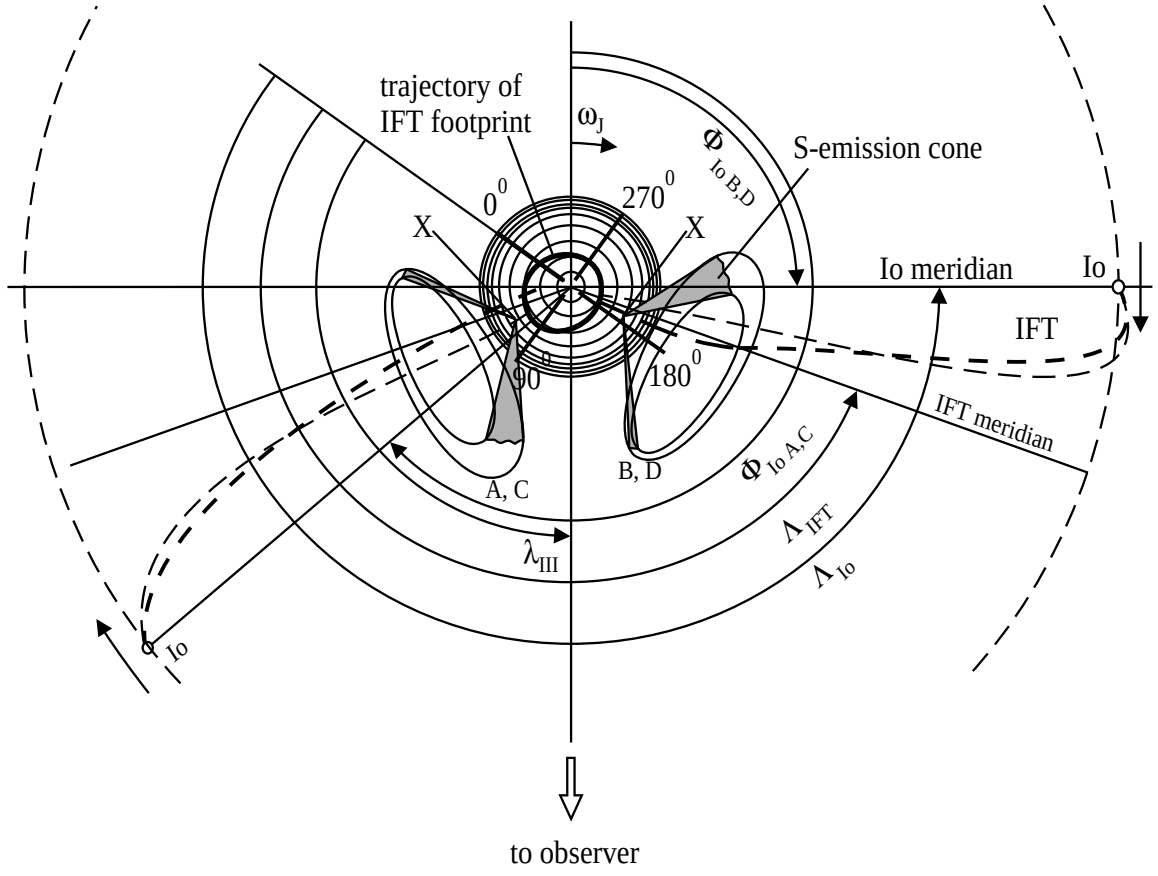

Figure 9: Jupiter–Io geometry relevant to S–emission, viewed from Jupiter's south pole. The hollow radio radiation cones of the decameter S–emission are represented at the two geometries corresponding to Io–AC and Io–BD sources, together with the corresponding Io meridian and IFT distorted geometry. Io's longitude (Λ_{Io}) is deduced from Io's phase (Φ_{Io}) and the observer's longitude (λ_{III}). In addition, the use of a magnetic field model (O6) allows to define the longitude (Λ_{IFT}) of the local IFT meridian at a given frequency (the source of which is denoted X on the Figure).

4 S–Emission Source Model

S–bursts generation can be interpreted in terms of self–organized critical phenomena, consistent with the recent radiation source model of Ryabov [1994], summarized below. As the Jovian magnetic dipole is tilted by about 10° on the planet's rotation axis and offset from its center by 0.1 R_J, it can be shown that the IFT base rotates with a non–uniform angular and linear velocity. In other words, the IFT base oscillates around the

uniformly rotating meridian of Io (see Figure 9). It may thus excite oscillations in the tube, propagating upwards (to Io) as Alfvén waves, and stimulating a long–duration pulse of electro–motive force at Io (em.f. pulse: $\Delta\vec{E}_{Io} = \int \Delta\vec{v} \times \vec{B}_J ds$). The pulse results in local increase of the tube current up to 10^8 A, and growth of the local magnetic field strength: a strong azimutal magnetic field $\vec{B}_T$ is produced by this current and adds to the Jovian field $\vec{B}_J$. The resulting vector sum $\vec{B}_S = \vec{B}_J + \vec{B}_T$ is a helical magnetic field around part of the IFT (Figure 10). Elementary helical current filaments at the surface layer of the IFT near Jupiter may break up abruptly, due to their enhanced intensity (up to 10^8 A) and to the increased IFT transverse velocity through the inner magnetosphere at "active" Jovian longitudes about 40° and 220°. A voltage $u_x = L\, di_x/dt$ is induced between the edges of disrupted helical filaments, corresponding to an electric field of local strength $E > 107$ V/m, which produces collective acceleration of phase–bunched radiating electrons to relativistic velocities. The velocity vector $\vec{v}_e$ of electron bunches is directed along the helical magnetic field $\vec{B}_S$. Also, the energy released at the disruption point ($W_L = L\, i_x^2/2$) can excite a fast magnetosonic wave propagating at the Alfvén velocity normally to the helical magnetic field $\vec{B}_S$ around the tube, and causing the rupture of adjacent current filaments. According to this scenario, one drifting S–burst is thus generated by a cascade disruption of adjacent current filaments. The magnetic tension of filaments on the tube surface (B_S^2/μ_0) varies inversely to the IFT section radius ($B_S \sim 1/r_T$). Thus, chain disruptions occur preferably at wider parts of the IFT, where stability of the surface current filaments is minimum, and they are inhibited at narrower places (r_T on Figure 10). S–bursts source regions are thus mainly distributed along IFT widenings (M_{xi} on Figure 10). Excitation of S–bursts generation at the base of the IFT stops when its transverse velocity drops under a critical level. The whole process starts again at the next active region or next rotation of Jupiter. The relativistic electron bunches moving along the magnetic field $\vec{B}_S$ produce coherent, linearly polarized relativistic curvature radiation (or magneto–drift radiation). Elliptical polarization is actually observed for the S–emission [Dulk et al., 1992], which may be reconciled with the above linear polarization, if, e.g., the emission sustains additional cyclotron–maser amplification (at the local gyrofrequency). The directivity of the relativistic magneto–drift radiation is a pencil–beam pattern directed along the bunch velocity vector $\vec{v}_e$. The rotation of this pencil beam due to the motion of electron bunches along the helical field $\vec{B}_S$ circling around the IFT, as well as post amplification through the cyclotron–maser mechanism, can finally produce the observed hollow cone pattern of S–emission (Figures 9 and 10). The asymmetry of cone walls may be simply explained by the curvature of the IFT axis with respect to the meridian plane [Ryabov, 1990b, 1992; Ryabov and Gerasimova, 1990].

Burst durations can be interpreted in terms of modulations of the IFT diameter along its axis (Figures 10 and 11). The existence of IFT widenings (or "bulbs") regularly distributed along its axis is supported independently by the persistent frequency dependence of S–bursts occurrence probability (Figure 7). In addition, S–bursts lifetime estimates derived from the proposed IFT model are consistent with direct measurements of the S–bursts fine structure. According to the above scenario, if the initial current break–up occurs at an altitude lower than that of the maximum diameter of a tube bulb, the radio radiation produced there is of smaller intensity and higher frequency. This may explain

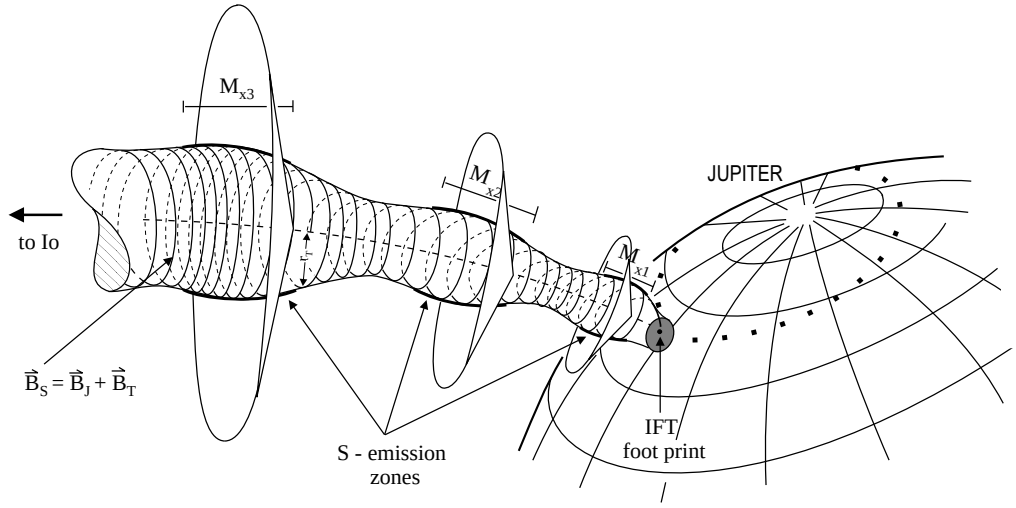

Figure 10: Sketch of S–emission source regions along the IFT upwards streaming branch (bulbs noted M_{xi} - see section 5). $\vec{B}_S$ is the helical surface IFT field. The trajectory of the IFT footprint at the surface of Jupiter is dotted.

the thin, weak upper frequency end of S–bursts of Figure 5.

The same consideration applies for lower frequency ends. The first stage of an S–burst storm as identified in observational data (simple quasi–linear bursts – see section 2 and Figure 1) may correspond to the early phase of IFT excitation, during which current filaments break, but the magnetic field topology is not yet strongly distorted. The next stage (more complex and intense bursts – Figures 2 through 4) would then correspond to the increasingly disturbed IFT field structure that results from cascade disruptions. The complexity of S–burst patterns is thus interpreted as a direct consequence of the complexity of the magnetic field lines and currents topology in or near the excited IFT.

5 Large–Scale Io Flux Tube Dynamics

Following the above model, the frequency width of S–burst sub–bands and their separation may be interpreted as the scale of bulbs along the IFT, i.e. as the size of regular widenings of the tube diameter of Io. Equivalently, the drift with time of the spectral sub–bands (section 2) can be interpreted in terms of slow bulb motions along the IFT. Finally, sub–bands width variations correspond to changes in the bulb extent as they move along the IFT. The sub–bands structure of the S–emission could thus be considered as a tracer of the large–scale dynamics of the IFT. If S–bursts generation occurs at the local electron gyrofrequency, the characteristic size M_x and velocity v_b of each bulb can be deduced from dynamic spectral observations (such as Figure 6). Using an empirical expression for the altitude h (km) of the S–radiation source in the IFT as a function of the emitted frequency f (MHz) [Ryabov, 1992]:

$$h \approx 1.46 \cdot 10^6 f^{-1.44}$$

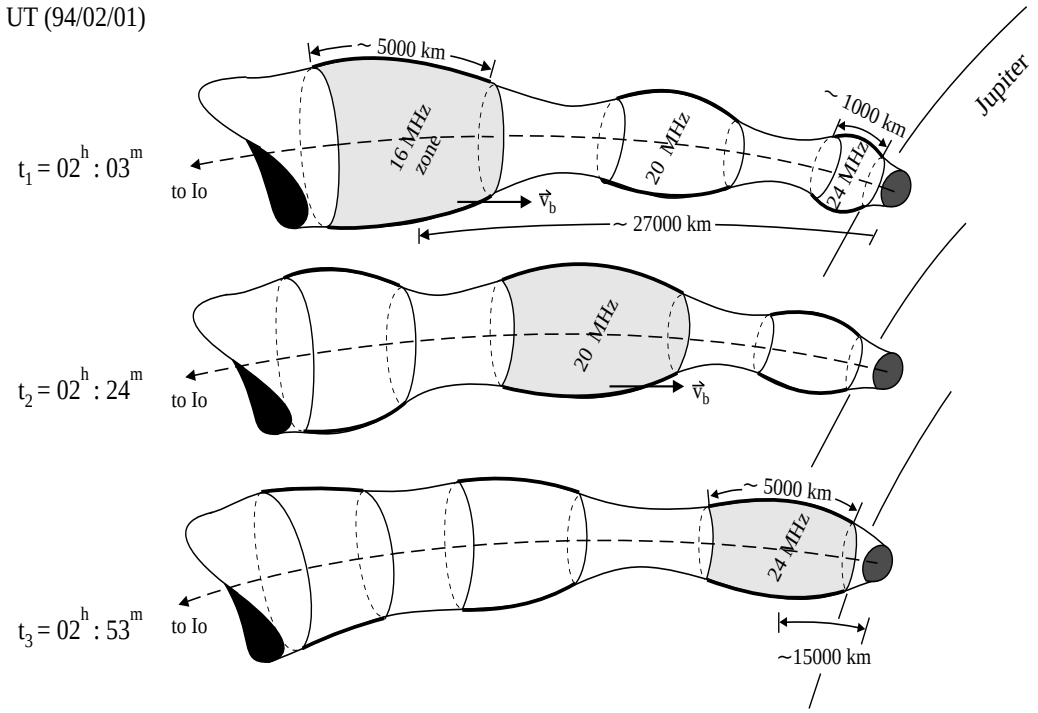

Figure 11: Sketch of the evolution of the IFT large–scale geometry during the S–bursts storm of February 1, 1994. The 4 MHz–wide sub–band drifting at ≈ 1.4 kHz/s corresponds to an emission region of parallel extent $M_x \approx 5000$ km, moving towards the planet's surface at an average velocity v_b of about 3 km/s. The change in the bandwidth of the 24 MHz sub–band during the same interval corresponds to a size variation of the corresponding source region from 1000 to 5000 km.

one can deduce v_b as:

$$v_b = \frac{dh}{dt} = \frac{dh}{df}\frac{df}{dt}_{sb} \ .$$

The above observed sub–band drift $(df/dt)_{sb} \approx 1.4$ kHz/s implies thus an overall source motion at $v_b \approx 2 \div 4$ km/s towards the planet's surface. Similarly, the size M_x (km) of the widening zone corresponding to a given observation writes [Ryabov, 1992]:

$$M_x = \frac{dh}{df}\Delta f \approx 2.1 \cdot 10^6 \, f^{-2.44} \Delta f \ ,$$

where Δf is the sub–band spectral width (or equivalently the total bandwidth of a typical S–burst in the sub–band). For example, the evolution of the IFT large scale geometry during the S–burst storm of 94/02/01 (examples of which are displayed in Figure 6) is illustrated on Figure 11. The 4 MHz–wide sub–band drifting from about 16 to 24 MHz in 50 minutes corresponds to an emission region of parallel extent $M_x \approx 5000$ km, moving towards the planet's surface at an average velocity $v_b \approx 3 \div 4$ km/s.

6 Recurrent, Scale–Invariants Fine Structure of S-Bursts

The signal amplitude within narrow S–burst sub–bands is generally smaller than in broad sub–bands, as illustrated on the 3–D spectra (amplitude–f–t) of Figure 12. If this proves to be a general characteristic of sub–bands, it could be explained invoking the size of the emitting zone in the IFT: as the evolution of an S–burst presumably results from the development of a local plasma instability along the IFT, a longer lifetime may imply a larger amount of released energy, and it corresponds to a more extended source region and thus a broader sub–bands spectral width. Sometimes, very intense bursts are observed across the spectral gap between adjacent sub–bands (between 20 and 24 MHz on Figure 13), which thus merge. The total bandwidth of the broadest bursts can then reach 7 MHz. These bursts may correspond to disruptions occasionally extending beyond the normal S–emission zones (M_{xi}), with the rupture point moving across the saddle–shaped region of Figures 10 and 11. A very interesting observational fact concerning the formation of f–t images in the IFT is the repetition of similar f–t patterns within short time–intervals. The typical separation of such fine structures is of the order of the duration of the pattern itself. Complex images appear thus in the f–t plane from 2 to 10 times within a few seconds. A typical example is displayed in Figure 14. This suggests that (quasi–)stable structures could exist in the IFT magneto–plasma (localized plasma density enhancements or depletions, magnetic field inhomogeneities, acceleration regions...), with a lifetime about one order of magnitude longer than a single S–burst. These structures could be able to radiate series of quasi–identical bursts. In addition, self-similar individual patterns also occur during different burst storms, separated by up to several years, as shown in Figure 15. While generating S–bursts, small perturbations of the IFT lead to cascades of energy releases. Such phenomena are usually attributed to the concept of self–organized criticality, commonly found in complex systems, suggesting that the IFT is in a state close to critical. In such systems, dynamics of equal complexity may appear at different spatial scales, which translates in the case of the IFT in similar patterns appearing on dynamic spectra with different f–t scales. Such occurrences are shown on Figure 16. Other examples of repetitive individual S–burst f–t patterns are given in Figures 17 through 21. If S–bursts are indeed emitted according to the above model, i.e. resulting from ruptures of current filaments at the surface of the flux tube of Io, then every elementary filament disruption should correspond to a small patch or dot of radio emission in the f–t plane (emission at a given time and a given frequency). The fact that S–bursts are generally observed as quasi–continuous patterns suggests that dots due to adjacent filament ruptures usually merge on the dynamic spectra. However it may happen, possibly when the tubes topology is strongly distorted, that only the brightest dots on the dynamic spectra are observable. Such peculiar occurence of a dotted S–bursts dynamic spectrum is shown on Figure 22. A schematic sketch of repetitive Jovian S–bursts f–t patterns that have been clearly identified in our data is given in Figure 23. Each of the displayed patterns may appear at different amplitude–time–frequency scales, i.e. they possess the property of three–dimensional scale invariance.

a)

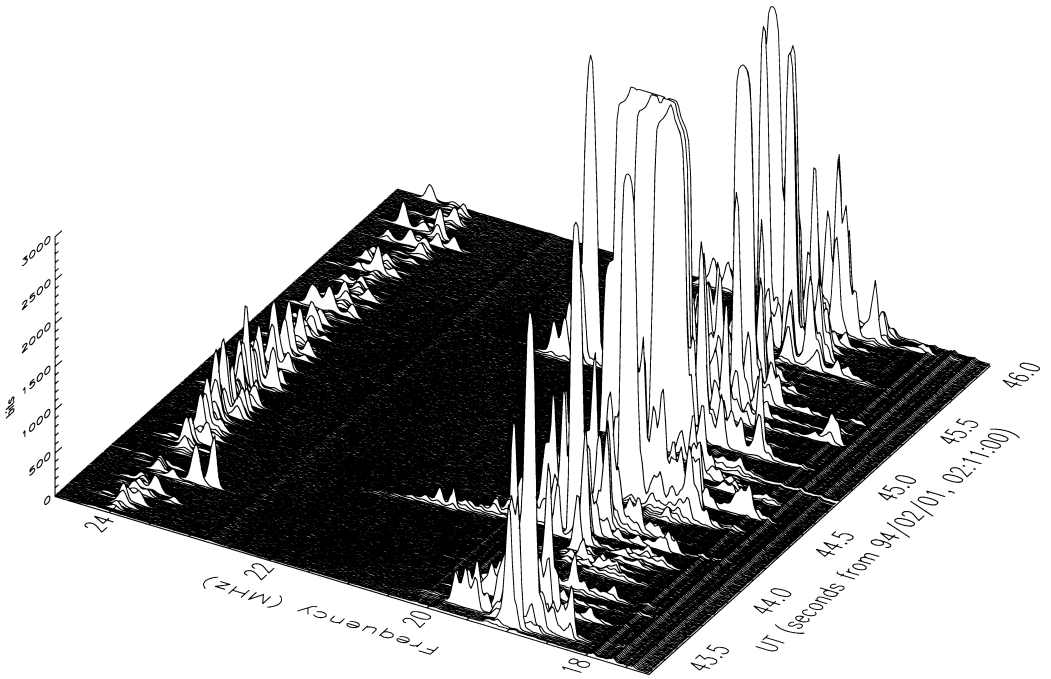

b)

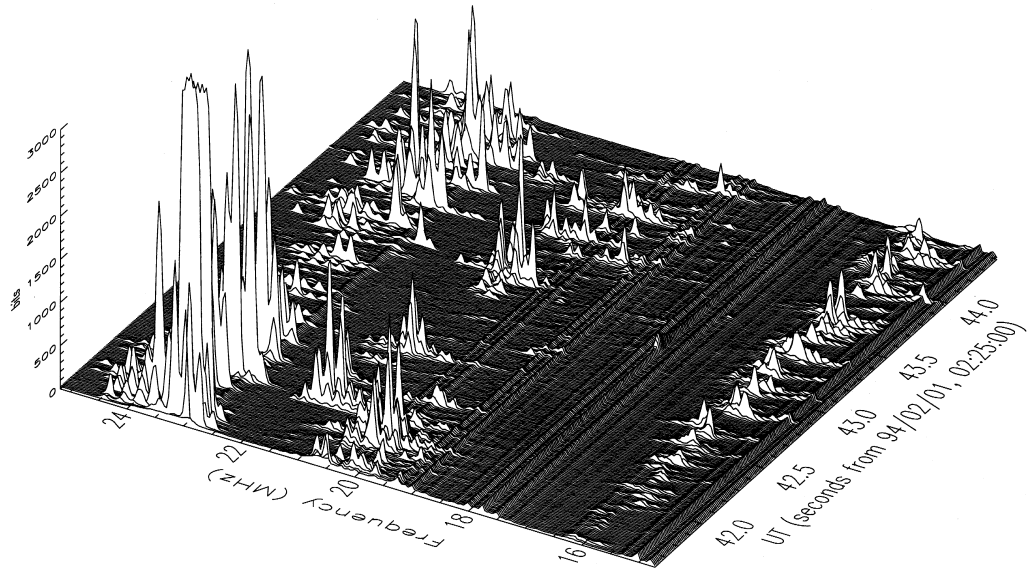

Figure 12: 3–D (raw amplitudes – frequency – time) plots of dynamic spectra of the Jovian Io–B S–emission recorded with UTR–2 + AOS on Feb. 1, 1994 (same as Figure 6). Two sub–bands are observed in a), *made of narrowband weak bursts at high frequencies (24 MHz) and broadband intense bursts – sometimes saturating – at low frequencies (20 MHz). 14 minutes later* b), *both the bandwidth and intensity of bursts about 24 MHz have much increased, while those of bursts about 20 MHz have decreased, and narrowband weak bursts appear around 16 MHz.*

a)

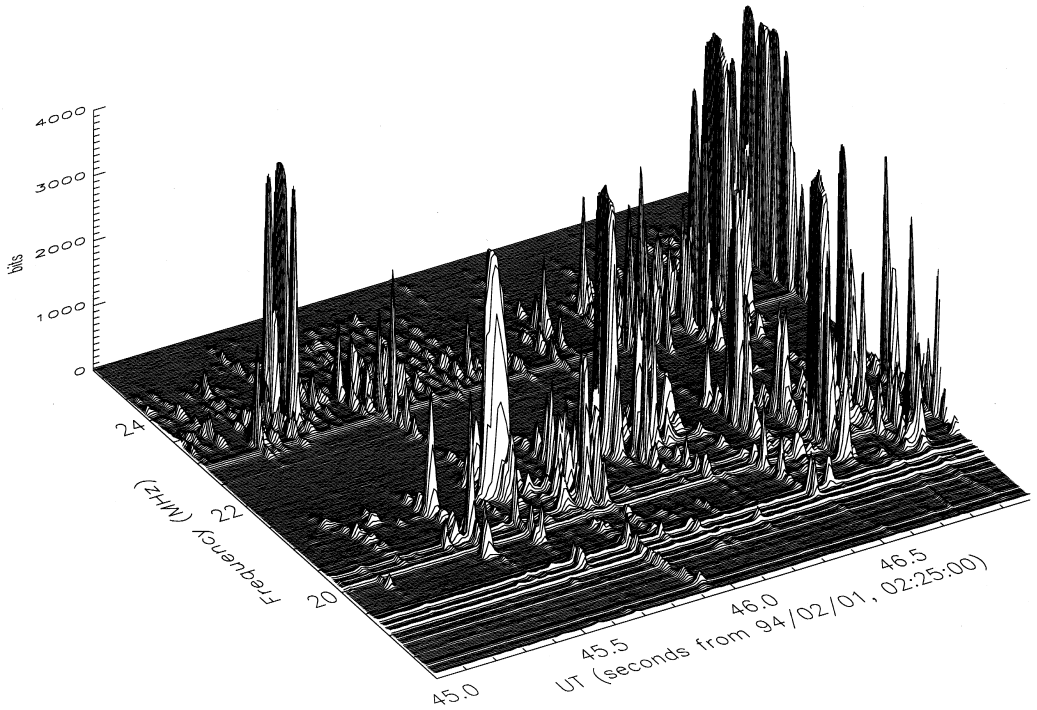

b)

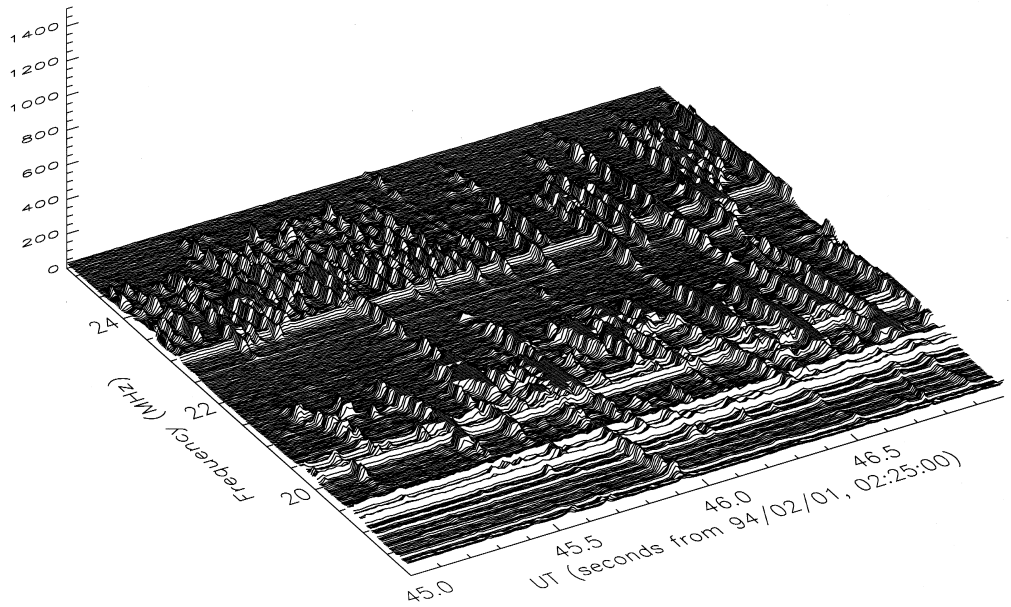

Figure 13: 3–D dynamic spectrum immediately following the one of Figure 12b (and corresponding to the upper 2 sub–bands of the end of Figure 6b). a) shows powerful individual bursts crossing the spectral gap between the sub–bands at 20 and 24 MHz. They are still better visible in b) which displays the same data with an upper amplitudes threshold about 100 data points (in the original 0 ÷ 4095 data points scale).

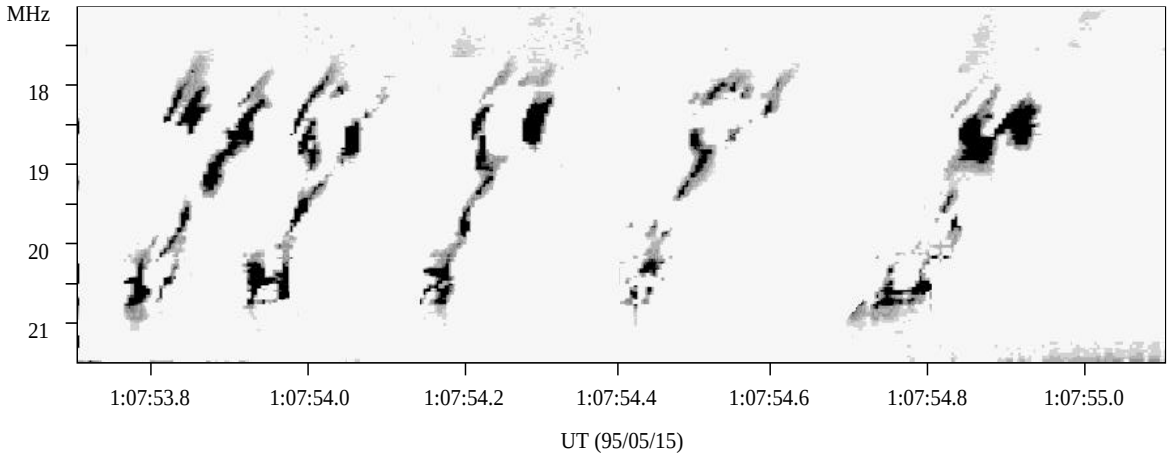

Figure 14: Recurrent quasi–periodic individual S–bursts patterns in AOS dynamic spectra recorded on May 15, 1995 (immediately prior in time with regard to Figure 3). The repetitive y–shaped structure (arrowed as in Figure 3) has been isolated from the surrounding emission.

7 Conclusions

New data collected from 1994 to 1996 using the high sensitivity UTR–2 array equipped with a high f–t resolutions AOS and a superfast digital MCS, allowing for broadband (>10 MHz) long–lasting (hours) observations, are presented and analyzed. They enabled us to uncover several new features of the Jovian S–emission, related to the evolution of the S–bursts fine structure during storms. Most of the observed features can be interpreted in the frame of the S–bursts generation model proposed by Ryabov [1992, 1994], in which the bursts are the final product of ruptures of small–scale current filaments circling around the IFT surface. The main results are:

1. The most versatile morphology of S–bursts f–t patterns corresponds to the Io–C source, whereas the Io–B source generates the most powerful and comparatively simple bursts. This can be attributed to the different geometries of the radio radiation beam with respect to the observer (Io–C corresponds to the observer facing the concave side of the IFT, and Io–B to the observer facing the convex side), and to the IFT footprint motion in Jupiter's inner magnetosphere. Two stages of increasing complexity are generally observed during storms. Well–organized patterns are however uncommon, and the S–bursts dynamic spectra are often made of random–like patterns.

2. S–bursts are often distributed within well–separated frequency sub–bands. The sub–bands occurrence maximizes around certain frequencies (13, 16.5, 20, 23.5 and 27 MHz). Fluctuations or drifts of the center frequency of a given sub–band are however observed at timescales of tens of seconds to minutes, with up to 1.5 MHz amplitude. Their bandwidth may also vary considerably (from 1 to 6 MHz) at a slower timescale (tens of minutes). These features are interpreted in terms of the large–scale dynamics of the IFT, identifying S–emission regions with variable and moving IFT widenings (bulbs). For example, the slow positive sub–band frequency

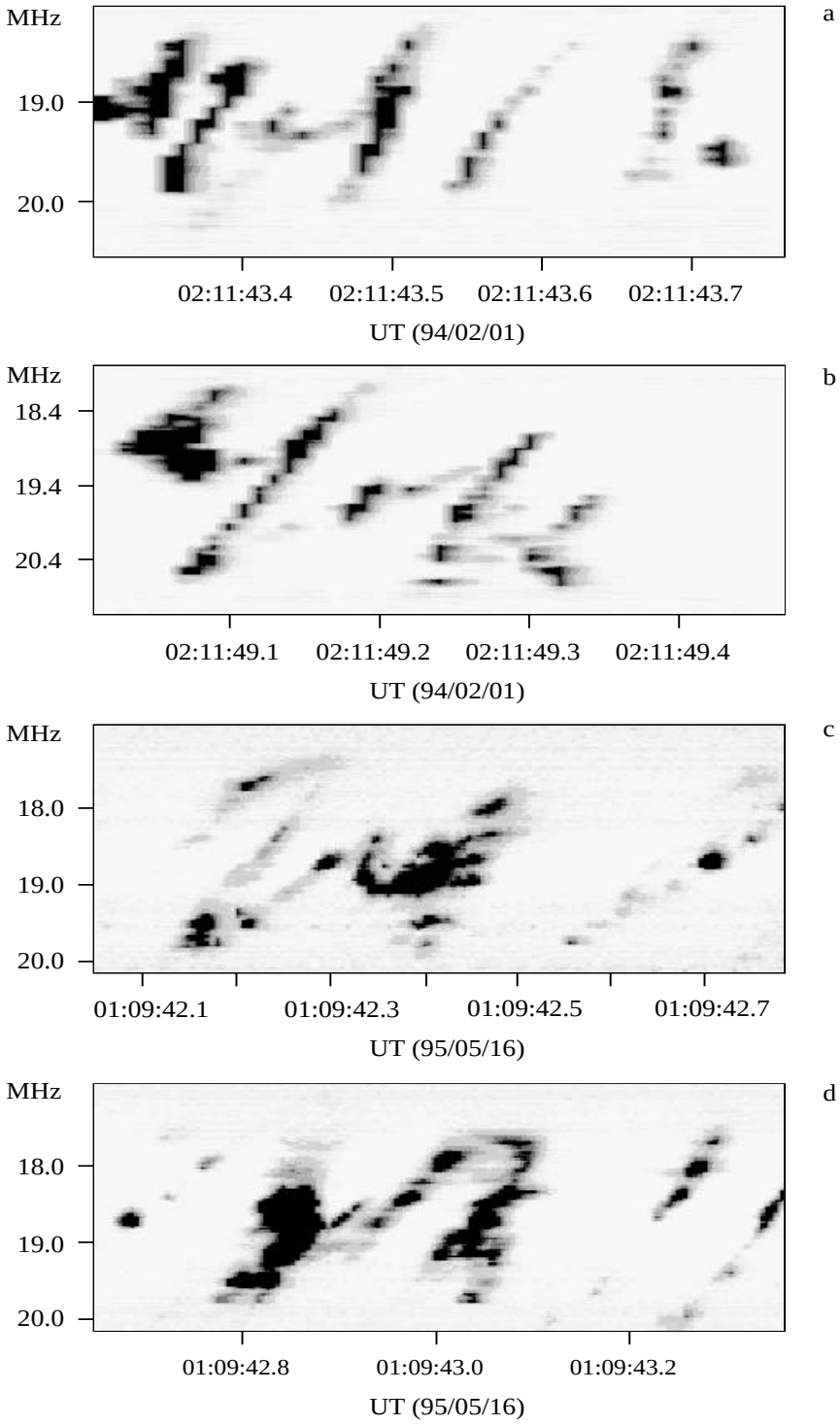

Figure 15: Complex, similar S–burst patterns in the f–t plane, recurrent in Io–B storms and separated by >15 months (February 1, 1994 (a,b) and May 16, 1995 (c,d)).

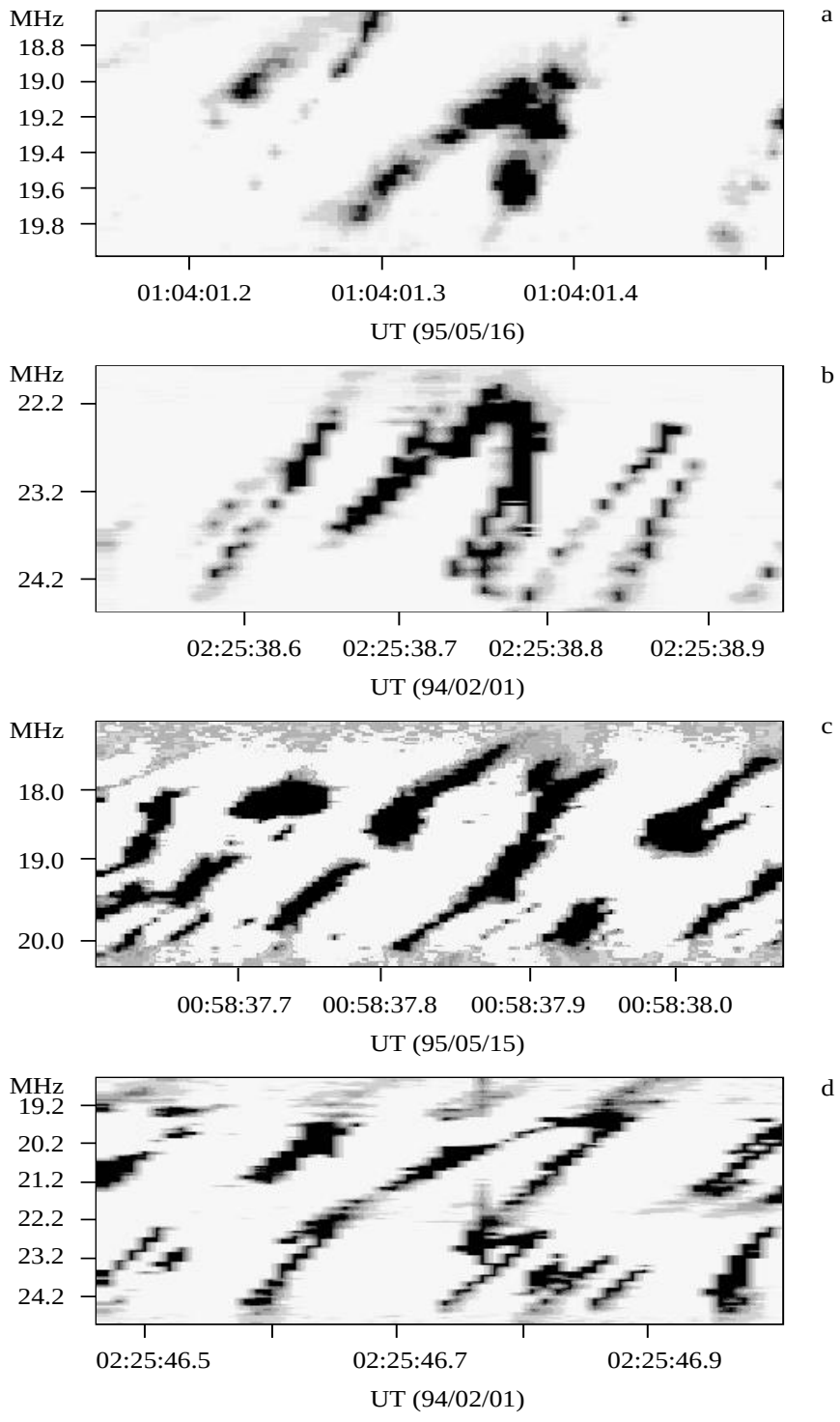

Figure 16: Self–similar S–burst patterns observed with different scales in the f–t plane, for Io–B emissions (February 1, 1994 (b,d) and May 16, 1995 (a)), as well as Io–C emissions (on May 15, 1995 (c)). The self–similarity (homothetic) factor is approximately proportional to the spectral width of the frequency sub–bands in which the bursts occur.

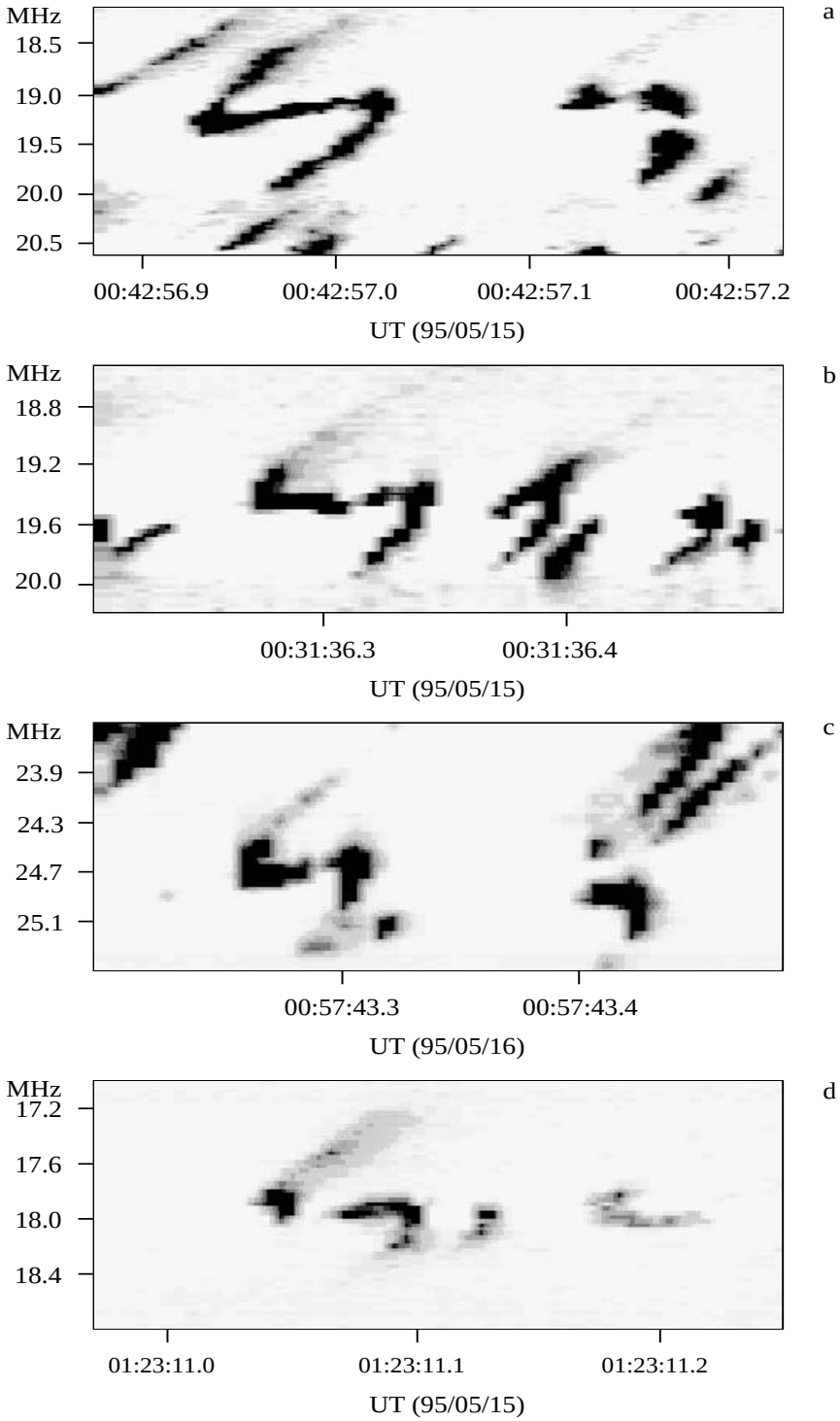

Figure 17: Recurrent S–shaped fine structure, often appearing with various amplitude–f–t scales in Io–B (c) and Io–C (a,b,d) dynamic spectra of S–emission.

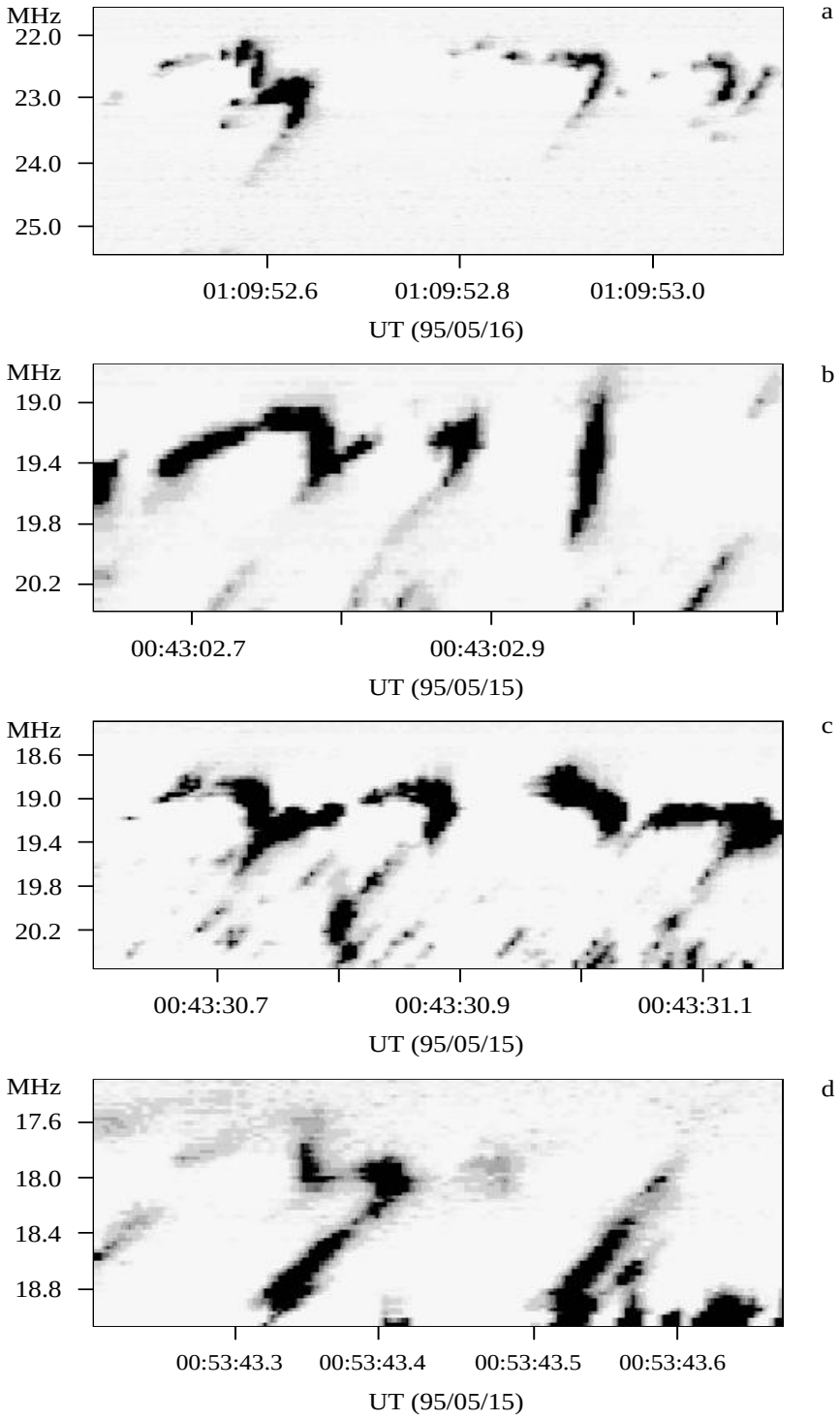

Figure 18: Recurrent m–shaped fine structure, with smooth transition from negative to positive frequency drift, in Io–B (a) and Io–C (b,c,d) dynamic spectra.

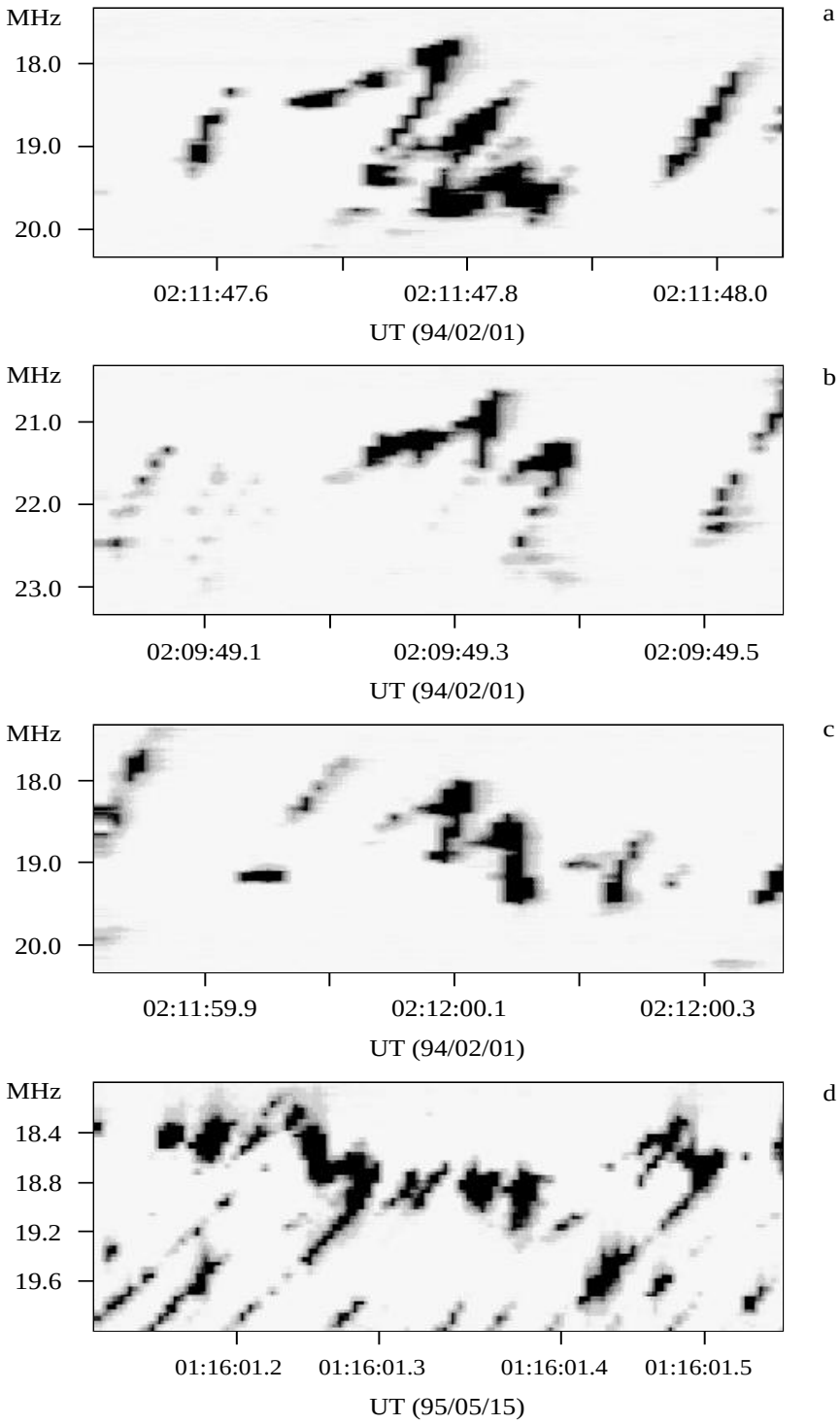

Figure 19: Recurrent reversed W–shape (somewhat similar to that of Figure 18), evidencing the occurrence of several different drift–rates (generally negative) at the same emission frequency.

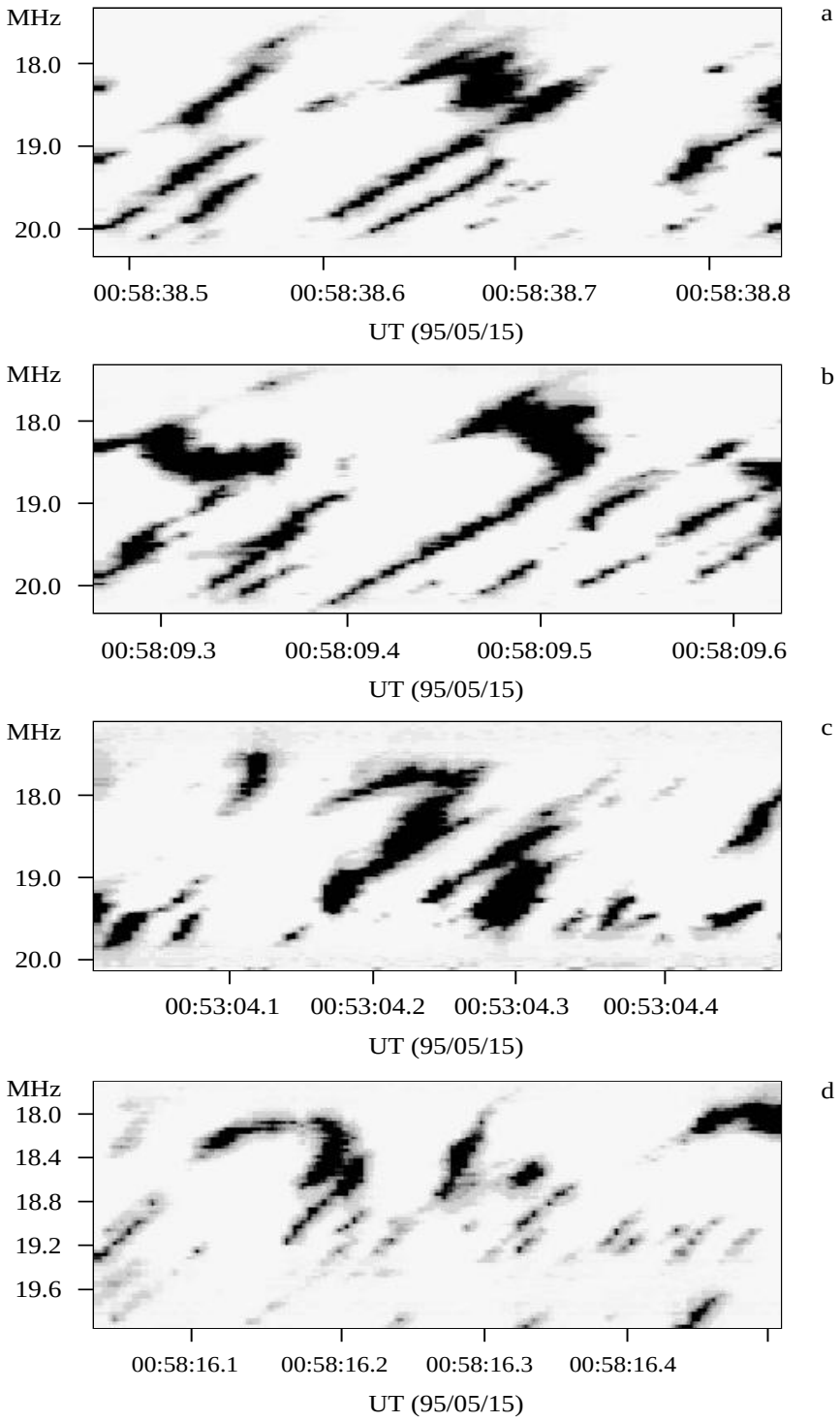

Figure 20: Complex fine structures with simultaneous positive and negative drift–rates (Io–C emission of May 15, 1995).

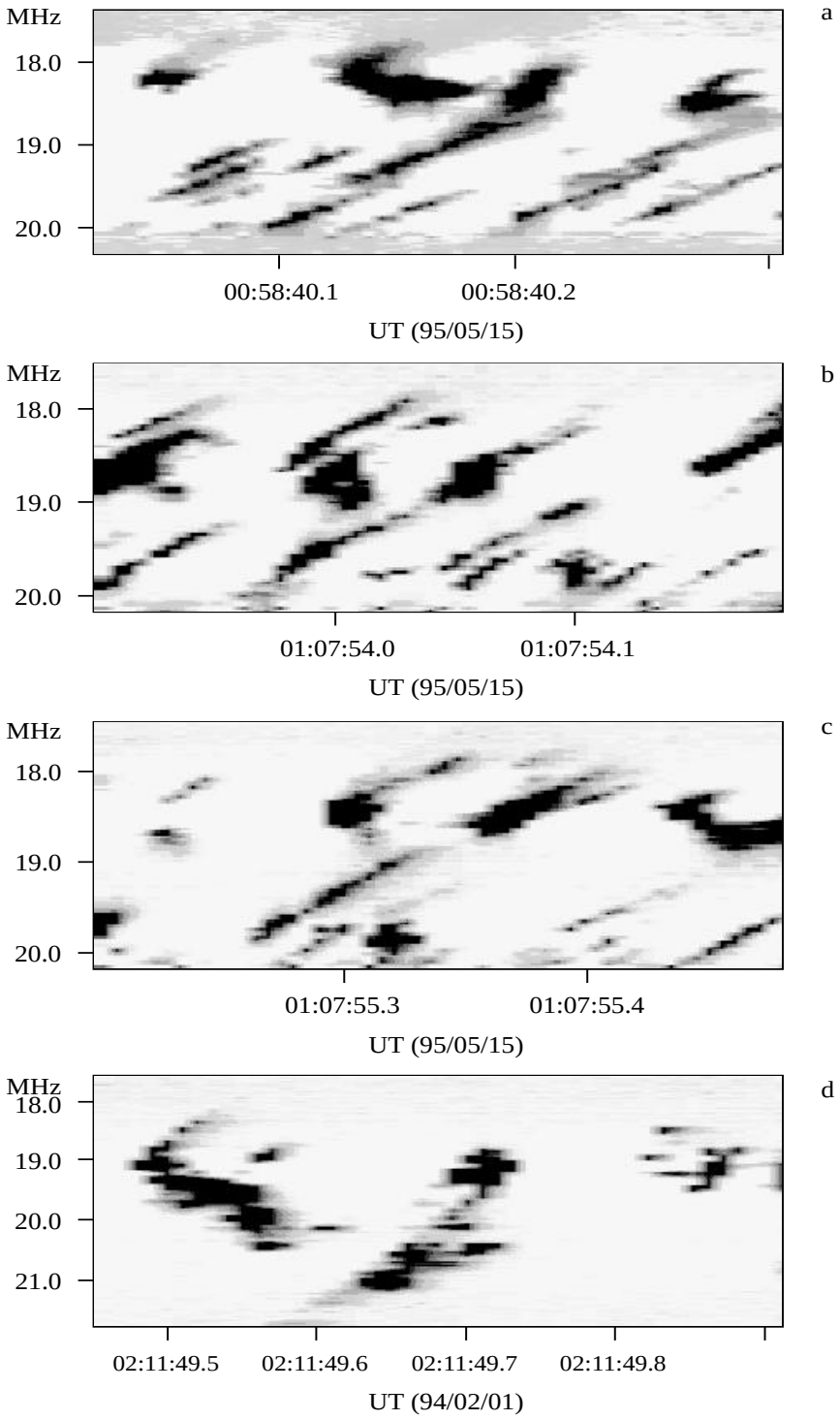

Figure 21: Distorted y–shaped structure (same as in Figure 14, Io–C emission of May 15, 1995), also recorded on Feb. 1, 1994 (Io–B). On May 15, 1995, recurrent self–similar patterns of this type were recorded up to 10 times within about 3 seconds.

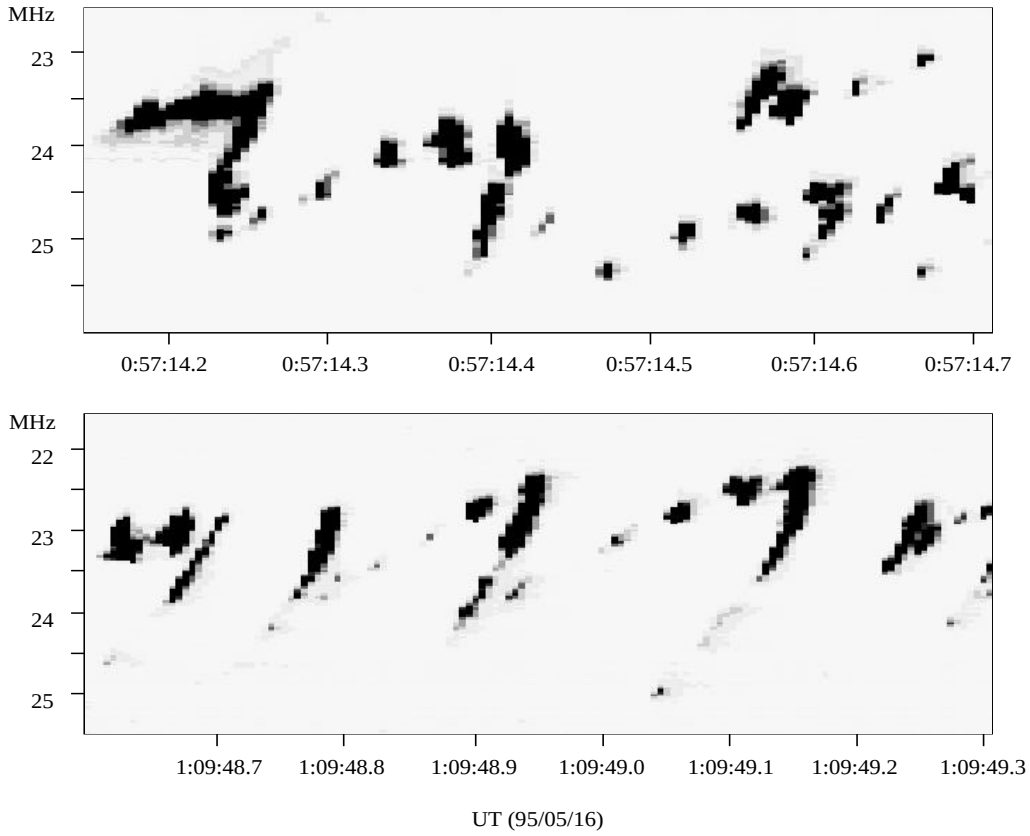

Figure 22: Intermittent S–bursts, appearing as dotted patterns on dynamic spectra (Io–B emission of May 16, 1995), and possibly associated to a strongly distorted topology of the IFT magnetic field and associated currents.

drift observed on 94/02/01 (1.4 kHz/s) can be interpreted as a motion of the corresponding source region along the IFT towards the planetary surface, at a velocity $v_b \approx 3 \div 4$ km/s.

3. Exceptionally intense bursts are sometimes observed to cross the spectral gap between bands. They may be interpreted as disruptions extending beyond the normal S–emission zones.

4. When observed with very high time resolution (MCS) and high sensitivity, the simplest, quasi–linear S–bursts reveal a clear stretched S shape. The fixed–frequency duration of a burst is substantially greater at its middle frequency than at its ends. This is attributed to the weaker efficiency of the burst generation at the edges of a source region.

5. The above negatively drifting S shape can be interpreted in terms of adiabatic motion of electrons in or near the IFT [Ellis, 1974; Zarka et al., 1996]. However, the S–bursts fine structure often exhibits complex patterns with positive drifts in close vicinity of negatively drifting details. This requires additional explanations.

6. The occasionally dotted shape of S–bursts in dynamic spectra is also consistent with

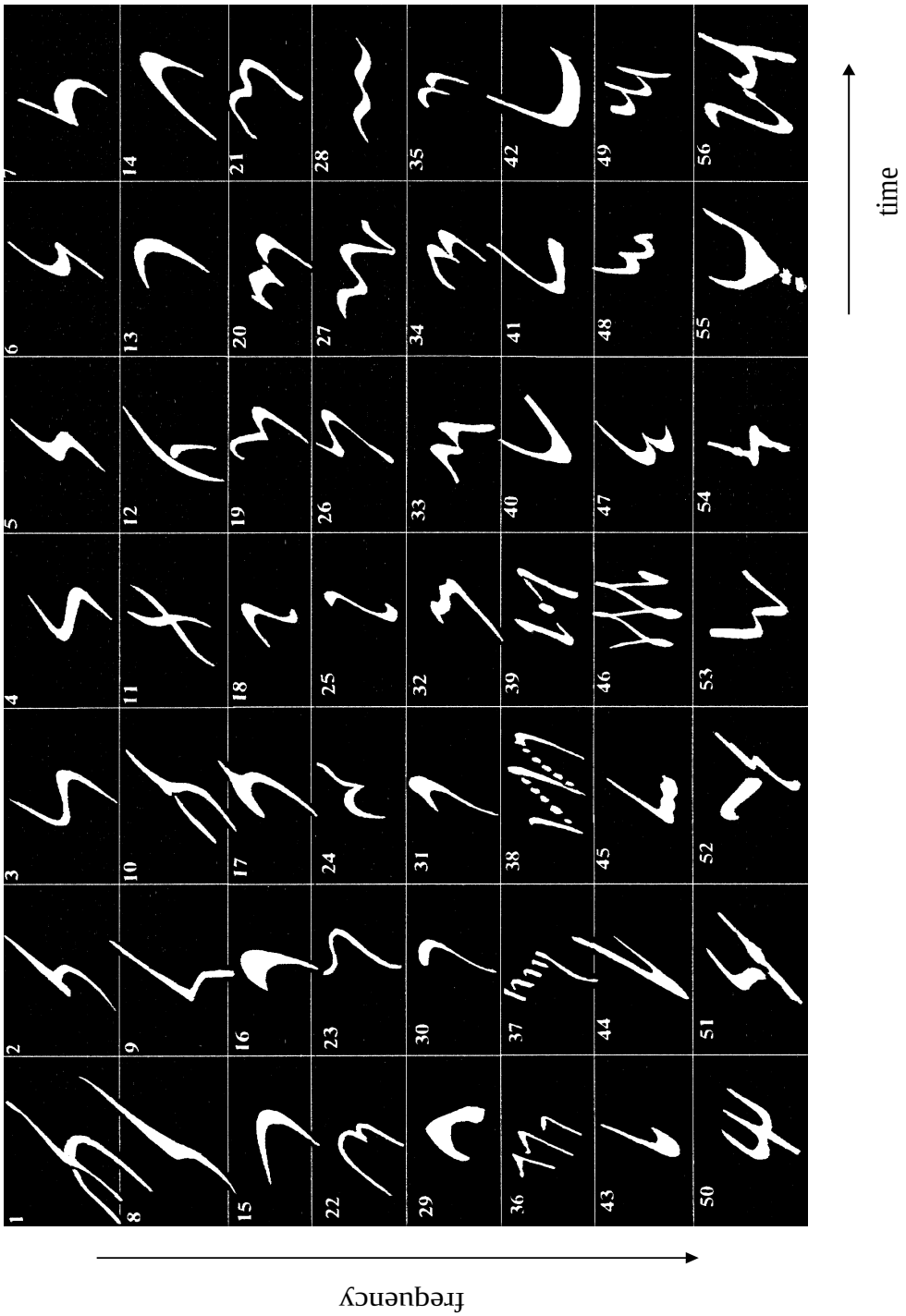

Figure 23: The S–bursts alphabet: sketch of Jovian S–bursts f–t patterns that have been repeatedly identified in our data between 1994 and 1996. They may appear at different amplitude–time–frequency scales (3–D scale invariance).

the proposed model, each dot corresponding to a single rupture event. Individual dots are usually merged in a quasi–continuous pattern due to the many adjacent ruptures along the IFT. However, they may become observable, possibly when the IFT topology is strongly distorted.

7. Complex S–bursts f–t patterns have been repeatedly observed (2 to 10 times) within time intervals of a few seconds, as well as in storms recorded during different years. In the latter case, these S–burst patterns may appear with different scales on the f–t plane. The self–similarity (homothetic) factor is then approximately the ratio of the spectral width of the sub–bands where these patterns appear. This property of similarity exists not only in the f–t domain, but also concerns S–bursts intensities: smaller patterns which occur in narrow sub–bands always have lower intensities.

8. Since the Io–Jupiter electric current system is non–uniformly distributed and probably sustains a complex spatial structure and temporal dynamics (variability), the evolution of an S–burst is probably related to the development of a plasma instability in the IFT. During S–burst generation, small perturbations of the IFT may trigger cascades of energy releases, which characterize a complex system close to (self–organized) criticality. This may be the underlying cause for the emergence of complex amplitude–f–t patterns at different scales, reflecting complex IFT dynamics at different spatial scales. As the scale of S–burst patterns on the f–t plane is defined by the geometric size of the generation region (in the frame of the above model), this 3–D scale invariance supports the direct dependence of the released energy with the dimension of the emitting region. The proposed interpretation of repeatable fine structures of S–burst emission in terms of self–organized criticality seems qualitatively consistent with the model developed for the radiation source, although more work is required to develop quantitative models of fine structures generation. Further observational investigation of superfine temporal and spectral structures of the Jovian S–burst emission are now required with extremely high sensitivity and time–frequency resolutions (0.5 ms and 10 kHz).

Acknowledgements: The authors acknowledge support from the E. C. INTAS program (contract for Joint Research Project # 94–1296). Further support was provided from Dieter F. Vogl for the preparation of the figures.